Jan W. Casselman, MD, PhD • F. Erwin Offeciers, MD, PhD • Paul J. Govaerts, MD
Rudolf Kuhweide, MD • Hugo Geldof, MD • Thomas Somers, MD • Guido D'Hont, MD

Aplasia and Hypoplasia of the Vestibulocochlear Nerve: Diagnosis with MR Imaging[1]

PURPOSE: To introduce aplasia or hypoplasia of the vestibulocochlear nerve (VCN) as a possible cause of hearing loss and to identify the magnetic resonance (MR) imaging characteristics of this entity.

MATERIALS AND METHODS: In seven patients with congenital deafness or unexplained sensorineural hearing loss, MR imaging enabled diagnosis of aplasia or hypoplasia of the VCN. Axial (0.7-mm) three-dimensional Fourier transformation–constructive interference in steady state (3DFT-CISS) images and parasagittal reconstruction images perpendicular on the course of the VCN were obtained. Twenty normal inner ears were also studied; their findings were compared with those of the patients.

RESULTS: The facial nerve and inferior and superior vestibular and cochlear branches of the VCN were identified on the MR images in the 20 normal inner ears. Aplasia of the VCN was detected in two patients with normal labyrinths but with a severe stenosis of the internal auditory canal. A common VCN with absence of the cochlear branch was found bilaterally in two patients with a congenital malformation of the labyrinth. A common VCN with absence or hypoplasia of the cochlear branch was found in three patients with normal internal auditory canals and labyrinths.

CONCLUSION: Submillimetric gradient-echo images (eg, 3DFT-CISS) should always be used to exclude aplasia or hypoplasia of the cochlear branch of the VCN in all cochlear implant candidates and patients with congenital deafness. This entity, which can occur with or without associated labyrinthine malformation, should be confirmed in two planes.

MAGNETIC resonance (MR) imaging is accepted as the method of choice to look for abnormalities in patients with sensorineural hearing loss and/or vertigo (1–5). Moreover, gradient-echo MR imaging proved its value in patients with congenital inner ear malformations (6) and especially in candidates for cochlear implantation (7–9). The MR demonstration of a normal cochlea, with a fluid-filled scala tympani and vestibuli, indicates that these patients are ideal candidates for implantation. Nevertheless, in some of these patients the cochlear implant did not result in auditory perception, although the implant itself worked and was not causing the problem (O'Donoghue GM, personal communication, 1996). A possible explanation could be an absent or abnormal cochlear branch of the vestibulocochlear nerve (VCN). With the advent of submillimetric T2-weighted gradient-echo images, these nerves and nerve branches can be visualized in a reliable way inside the internal auditory canal and cerebellopontine angle (10). In the internal auditory canal, the facial nerve and the cochlear branch, inferior vestibular branch, and superior vestibular branch of the VCN are best recognized on axial three-dimensional Fourier transformation–constructive interference in steady state (3DFT-CISS) images and can be confirmed on parasagittal reconstruction images (5).

The purpose of our study was to introduce aplasia or hypoplasia of the VCN as a possible cause of sensorineural hearing loss or congenital deafness and to identify the MR imaging characteristics of this entity with use of the 3DFT-CISS sequence.

MATERIALS AND METHODS

Subjects

During a period of 24 months (from February 1994 to January 1996), the diagnosis of aplasia or hypoplasia of the cochlear branch of the VCN was made at MR imaging in seven patients (six male patients, one female patient; age range, 2–42 years; average age, 11 years). The common clinical finding that led to computed tomography (CT) and MR imaging was sensorineural hearing loss. The sensorineural hearing loss was congenital and bilateral in three patients (who were part of a cochlear implantation selection program) and congenital and unilateral in three patients, and sudden hearing loss occurred in one patient. More details of the clinical presentation of these patients are listed in the Table.

Imaging Protocol

All patients underwent MR imaging performed with a 1-T, active-shielded su-

Index terms: Ear, abnormalities, 125.1419, 125.1429 • Ear, anatomy, 125.92 • Ear, MR, 125.121412 • Magnetic resonance (MR), pulse sequences, 125.121412 • Magnetic resonance (MR), thin section, 125.121412 • Nerves, abnormalities, 125.1419, 125.1429

Abbreviations: 3DFT-CISS = three-dimensional Fourier transformation–constructive interference in steady state, VCN = vestibulocochlear nerve.

Radiology 1997; 202:773–781

[1] From the Departments of Diagnostic Radiology (J.W.C.) and Otorhinolaryngology (R.K., G.D.), AZ St-Jan Brugge, Ruddershove 10, B-8000 Brugge, Belgium; the University Department of Ear, Nose and Throat, Sint-Augustinus Hospital, University of Antwerp, Belgium (F.E.O., P.J.G., T.S.); and the Department of Otorhinolaryngology, AZ St-Lucas, Brugge, Belgium (H.G.). Received June 14, 1996; revision requested July 29; revision received October 10; accepted October 14. **Address reprint requests to** J.W.C.
© RSNA, 1997

Clinical and Imaging Data of the Affected Inner Ears of the Seven Patients with Aplasia or Hypoplasia of the VCN

Patient No./Sex/ Age (y)	Clinical Presentation	Side	CT Findings	MR Findings		
				Labyrinth	IAC	Nerves
1/F/2	Until age 9 months, parents thought the child had normal hearing; at 14 months, bilateral congenital deafness was confirmed with audiogram (vibration deafness) and ABR; normal facial nerve function; potential cochlear implant candidate	Right	IAC stenosis	Normal	Stenosis	Aplasia of VCN
		Left	IAC stenosis	Normal	Stenosis	Aplasia of VCN
2/M/42	Bilateral aplasia of external ear and the EAC, normal facial nerve function, plastic and otologic surgery (approximately 30 interventions), BAHA on the right side and bilateral epitheses, sudden SNHL on the right side (at age 42 years) with completely deaf ear on the left (per audiogram)	Left	Stenosis, separate canal for facial nerve	Normal	Stenosis, separate canal for facial nerve	Aplasia of VCN
3/M/2	Congenital deafness, noted by parents at age 6 months; at 18 months, deafness confirmed with ABR and audiogram (corner audiogram); presumably autosomal or X-linked recessive; electric promontory stimulation: response on left ear; potential cochlear implant candidate	Right	Common cavity, abnormal semicircular canals	Common cavity, abnormal semicircular canals	Normal	Common VCN
		Left	Common cavity, abnormal semicircular canals	Common cavity, abnormal semicircular canals	Normal	Common VCN
4/M/10	Bilateral congenital deafness confirmed with audiogram; electric promontory stimulation is planned; potential cochlear implant candidate	Right	Common cavity, IAC stenosis, partial development of SSC	Common cavity, partial development of SSC	Stenosis	Common VCN
		Left	Common cavity, IAC stenosis, partial development of SSC	Common cavity, partial development of SSC	Stenosis	Common VCN
5/M/6	Congenital hearing loss on the left side since birth; at 6 years, total congenital deafness on the left side confirmed with audiogram (phantom curve), normal hearing on the right side	Left	Normal	Normal	Normal	Rudimentary vestibular nerve, absent cochlear branch
6/M/5	Congenital deafness on the right side since birth, only mild hearing loss on the left; completely deaf ear on the right confirmed with audiogram	Right	Not applicable	Normal	Normal	Rudimentary vestibular nerve, absent cochlear branch
7/M/12	Child turns head to the left to hear with normal right ear; congenital high frequency hearing loss on the left side confirmed with audiogram; normal hearing on the right	Left	Normal	Normal	Normal	Hypoplasia of the cochlear branch

Note.—ABR = auditory brain-stem responses, BAHA = bone-anchored hearing aid, EAC = external auditory canal, IAC = internal auditory canal, SNHL = sensorineural hearing loss, SSC = superior semicircular canal.

perconductive system (Magnetom SP 42; Siemens, Erlangen, Germany). A standard circular polarized head coil was used to allow simultaneous imaging of both inner ears. All patients underwent a routine inner ear study with an axial, 7-mm-thick, T2-weighted spin-echo sequence (2,000/16, 90 [repetition time msec/echo time msec], one signal acquired) of the brain and a selective, axial, 3-mm-thick, contiguous, T1-weighted spin-echo sequence (500/14, four signals acquired) with and without administration of an intravenous gadolinium chelate. Their temporal bones were also examined with a coronal gadolinium-enhanced T1-weighted sequence. A dose of 0.1 mmol/kg gadoterate meglumine (Dotarem; Guerbet Laboratories, Aulnay-sous-Bois, France) or gadopentetate dimeglumine (Magnevist; Schering, Berlin, Germany) was used. The patients were also examined with a 3DFT-CISS gradient-echo sequence. The details of this gradient-echo sequence have been published previously (4,10). The most important parameters of this sequence are the following: 15/21, 65° flip angle, one axial slab of 22.4-mm thickness, 32 partitions, 256 × 256 matrix, 170-mm field of view, two signals acquired. This results in 0.7-mm axial sections with an in-plane resolution of 0.66 × 0.66 mm and a total acquisiton time of 8 minutes 6 seconds. The absence of nerves or nerve branches was always checked on parasagittal 3DFT-CISS reconstruction images. These reconstruction images were made through the cerebellopontine angle and middle and lateral thirds of the internal auditory canal and were angled perpendicular on the course of the nerves (Figs 1, 2a, 2b).

In six of the patients, 1.5-mm-thick axial CT sections also were obtained every 1 mm, and in two patients (patients 2 and 4) additional coronal CT scans were acquired.

Control Group

Twenty normal inner ears were also studied with 0.7-mm-thick 3DFT-CISS images. The selected 3DFT-CISS examinations were free of movement or flow artifacts and therefore allowed adequate evaluation of the nerves in the cerebellopontine angle and internal auditory canal. The reliability to distinguish the facial nerve and the inferior vestibular, superior vestibular, and cochlear branches of the VCN in the cerebellopontine angle and internal auditory canal was checked on these axial images and on the parasagittal 3DFT-CISS reconstruction images, made

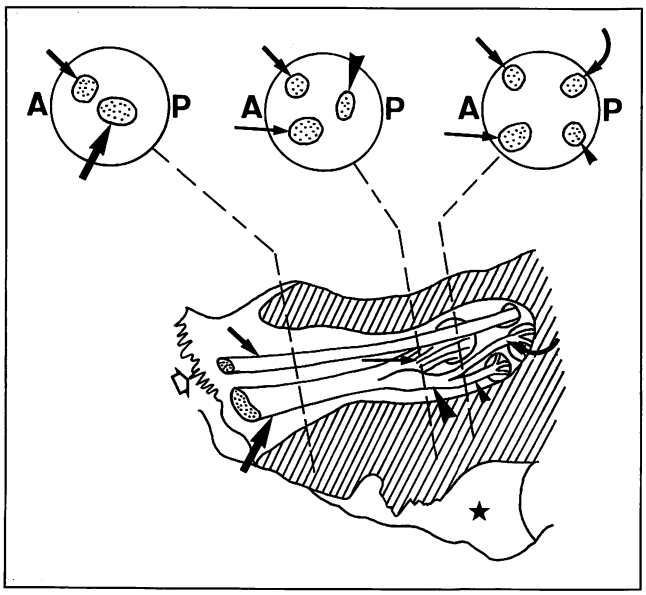

Figure 1. Diagram shows the nerves in the internal auditory canal. The posterior wall of the internal auditory canal is removed, and cross sections (top) through the cerebellopontine angle–porus region (left), middle third of the internal auditory canal (middle), and lateral third of the internal auditory canal (right) were made. Facial nerve (small thick arrow), VCN (large arrow), common vestibular nerve (large arrowhead), inferior vestibular branch (small arrowhead), superior vestibular branch (curved arrow), and cochlear branch (thin arrow) of the VCN are indicated. *A* = anterior, *P* = posterior, ★ = jugular foramen, open arrow = petro-occipital fissure.

perpendicular on the course of the nerves in the cerebellopontine angle and in the middle and lateral thirds of the internal auditory canal. The thickness of the nerves in relation to one another was evaluated on the parasagittal reconstruction images. Especially, the thicknesses of the VCN (in the cerebellopontine angle) and its cochlear branch (in the internal auditory canal) were compared with the thickness of the facial nerve.

RESULTS

Control Group

The facial nerve and the cochlear branch, inferior vestibular branch, and superior vestibular branch of the VCN (Fig 1) could be visualized on the axial 3DFT-CISS images in all 20 normal inner ears (Fig 2a, 2b). On the parasagittal reconstruction images made at the level of the cerebellopontine angle, both the facial nerve and VCN were always visible. At this location, the VCN was 1½–2 times larger in diameter than the facial nerve in 19 of the 20 normal inner ears (Fig 2c). In one inner ear, they were the same size. In 19 inner ears, the facial nerve and the cochlear branch of the VCN and the common vestibular nerve (the vestibular branch of the VCN, not yet bifurcating into a superior and inferior branch) could be distinguished on the parasagittal reconstruction images made through the middle third of the internal auditory canal. The three branches of the VCN and the facial nerve could be separated from one another on the parasagittal reconstruction images made near the fundus of the internal auditory canal. In only one patient was it difficult to visualize the facial nerve because this nerve probably was small and adjacent to the wall of the internal auditory canal; the three branches of the VCN were clearly visible. On these images made through the internal auditory canal, the cochlear branch of the VCN was larger than the facial nerve in 12 inner ears, was as large as the facial nerve in five inner ears, and was smaller than the facial nerve in only three inner ears (Fig 2d, 2e).

Patients

In all patients, the T2-weighted spin-echo images of the brain were normal, and the unenhanced and gadolinium-enhanced T1-weighted images of the inner ear helped confirm only the stenosis of the internal auditory canal (five inner ears [three patients]) and the malformations of the osseous and membranous labyrinths (four inner ears [two patients]). However, these inner ear malformations were far easier to visualize on the 3DFT-CISS images. The absence of gadolinium enhancement in the cerebellopontine angle, internal auditory canal, and membranous labyrinth ruled out an acoustic neuroma or acute labyrinthitis as the cause of the deafness or hearing loss. Chronic labyrinthitis was ruled out on CT scans (no calcifications) and on the 3DFT-CISS images (no fibrous obliteration of the intralabyrinthine fluid spaces). Both inner ears were involved in three of the seven patients.

Two patients (three inner ears) had normal osseous and membranous labyrinths but had very narrow internal auditory canals. One of them (patient 2) even had a separate bony canal for the facial nerve, parallel to the internal auditory canal. In these two patients, the VCN was completely absent, and only a facial nerve was visualized on the gradient-echo images (Fig 3).

Associated malformations of the osseous and membranous labyrinths were seen in only two patients (four inner ears [patients 3 and 4]), and in one of them, the internal auditory canal was also stenotic on both sides. These patients had a common VCN, without trifurcation into cochlear, inferior vestibular, and superior vestibular branches (Fig 4).

Three other patients (three inner ears) had normal internal auditory canals and labyrinthine structures. Two of them (patients 5 and 6), however, had a common VCN running toward the vestibular labyrinth, and in both patients the cochlear branch of the VCN was absent (Fig 5). In the other patient (patient 7), hypoplasia of the cochlear branch of the VCN was found (Fig 6). All MR and CT findings are listed in the Table.

DISCUSSION

For years, CT was the best technique to look for congenital malformations of the inner ear in patients with congenital deafness. With the advent of MR imaging, it became possible to exclude abnormality along the acoustic pathway and in the auditory cortex on T2-weighted spin-echo images. Later on, gadolinium-enhanced T1-weighted spin-echo images were used in these patients to exclude acoustic neuromas, labyrinthitis, and other possible pathologic conditions in the cerebellopontine angle, internal auditory canal, and membranous labyrinth (1–5). In recent years, T2-weighted gradient-echo techniques have been used more and more to study the inner ear. These gradient-echo images are needed to evaluate the very small structures of the inner ear and to detect some of the abnormalities in the cerebellopontine angle, internal auditory canal, and membranous laby-

rinth (4–6,8). Good gradient-echo images must provide high contrast between the cerebrospinal fluid–intralabyrinthine fluid, nerves, and bone, and the sections must be very thin. In this study, axial 0.7-mm-thin 3DFT-CISS images were used because they provide excellent contrast between the different inner ear structures, and even the cerebrospinal fluid around the brain stem remains completely white on these images (10). Similar results were reported with other gradient-echo techniques, including 3D gradient-recalled acquisition in the steady state (11), contrast material–enhanced fast acquisition in the steady state (12), and 3D fast imaging with steady-state precession (13), and even a fast spin-echo (14) sequence proved to be beneficial in the study of the inner ear. The congenital malformations, detectable with CT, could now also be recognized on these gradient-echo images. The big advantage, however, was that it now became possible to detect unexpected inner ear malformations in patients with sensorineural hearing loss and/or vertigo by using MR alone, obviating an additional CT study (6).

CT and MR imaging could now be used to confirm the presence of a normal cochlea in candidates for cochlear implantation and to exclude calcifications in the cochlea (at CT) and/or fibrous obliteration in the membranous labyrinth (at MR imaging). In the absence of calcifications and fibrous obliterations, it is possible to introduce a cochlear implant into the cochlea. It is, however, obvious that the next important structure to be checked in these patients is the cochlear branch of the VCN. However, the MR technique must be fine-tuned to be useful for detection of nerve aplasias or hypoplasias. These malformations can be detected only on thin-section T2-weighted gradient-echo images (eg, 3DFT-CISS, etc) or comparable fast spin-echo images.

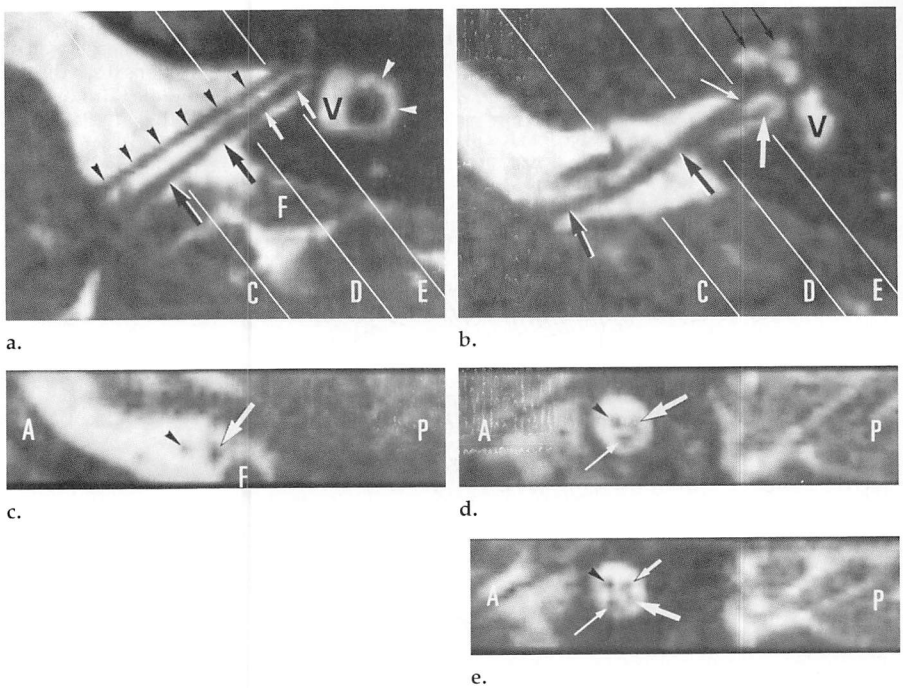

Figure 2. Normal facial nerve and VCN in the cerebellopontine angle and internal auditory canal. **(a)** Axial 0.7-mm-thick 3DFT-CISS image (15/21, 65° flip angle) obtained through the superior part of the left internal auditory canal shows the total course of the facial nerve (black arrowheads) from the brain stem to the fundus of the internal auditory canal. At this level, the facial nerve is always parallel to the VCN (black arrows), which becomes the superior vestibular branch (white arrows) of the VCN in the lateral part of the internal auditory canal. *F* = flocculus, *V* = vestibule, white arrowheads = lateral semicircular canal. **(b)** Axial 0.7-mm-thick 3DFT-CISS image (15/21, 65° flip angle) obtained through the inferior part of the left internal auditory canal. A typical bifurcation of the VCN into the cochlear (thin white arrow) and inferior vestibular (large white arrow) branches is always visible on the images through the inferior half of the internal auditory canal. The VCN can be seen in the cerebellopontine angle and medial third of the internal auditory canal (large black arrows). *V* = vestibule, thin black arrows = cochlea. Lines *C–E* represent the perpendicular lines along which the reconstruction images **c–e** were obtained. **(c)** Parasagittal 3DFT-CISS reconstruction image obtained perpendicular to the course of the nerves at the level of the cerebellopontine angle (along line C in **a** and **b**). The VCN (arrow) and the facial nerve (arrowhead) can always be recognized at the level of the cerebellopontine angle, and at this site the VCN is nearly always 1½–2 times larger in diameter. *A* = anterior, *F* = flocculus, *P* = posterior. **(d)** Parasagittal 3DFT-CISS reconstruction image obtained perpendicular to the course of the nerves at the level of the middle third of the internal auditory canal (along line D in **a** and **b**). The VCN has divided into a cochlear branch (thin white arrow) and a common vestibular branch (large white arrow). The facial nerve (arrowhead) is visible in its normal high and anterior position in the internal auditory canal. *A* = anterior, *P* = posterior. **(e)** Parasagittal 3DFT-CISS reconstruction image obtained perpendicular to the course of the nerves at the level of the lateral third of the internal auditory canal (along line E in **a** and **b**). Near the fundus of the internal auditory canal, the facial nerve (arrowhead) and the cochlear branch of the VCN (thin white arrow) are still visible in the anterior part of the internal auditory canal and have the same size, which can be normal, but more frequently the cochlear nerve is the larger one. At this level, the common VCN has split into superior (small white arrow) and inferior (large white arrow) branches. *A* = anterior, *P* = posterior.

Visualization of the Nerves in the Internal Auditory Canal

It is crucial to use images with a thickness of 1 mm or less to visualize the facial nerve and the three branches of the VCN separately inside the internal auditory canal. Nerve visualization becomes more accurate when, for instance, 0.7-mm-thick sections are used instead of 1.0-mm sections (10). The four nerves could be visualized in the internal auditory canal on the axial 0.7-mm-thick 3DFT-CISS images in all 20 normal inner ears and on the parasagittal reconstruction images in 19 of them. This proves that in the absence of movement artifacts, in cooperative patients, this technique is reliable enough to demonstrate the four nerves (Fig 2). Verification of the nerves in a second plane makes the technique even more reliable. It can also happen that a nerve is lying against the anterior or inferior wall of the medial part of the internal auditory canal, and in these patients the parasagittal reconstruction images can help in the demonstration of a nerve that is difficult to see on the axial images.

The thickness of the nerves inside the internal auditory canal can be measured, but these nerves are too small to be measured in a reliable way on images with an in-plane resolution of 0.66 × 0.66 mm and a thickness of 0.7 mm. The voxels are nearly isotropic or cubically shaped when these in-plane and section-thickness dimensions are used, and the use of such voxels will result in good quality multiplanar reconstruction images. The diameter of the common vestibular

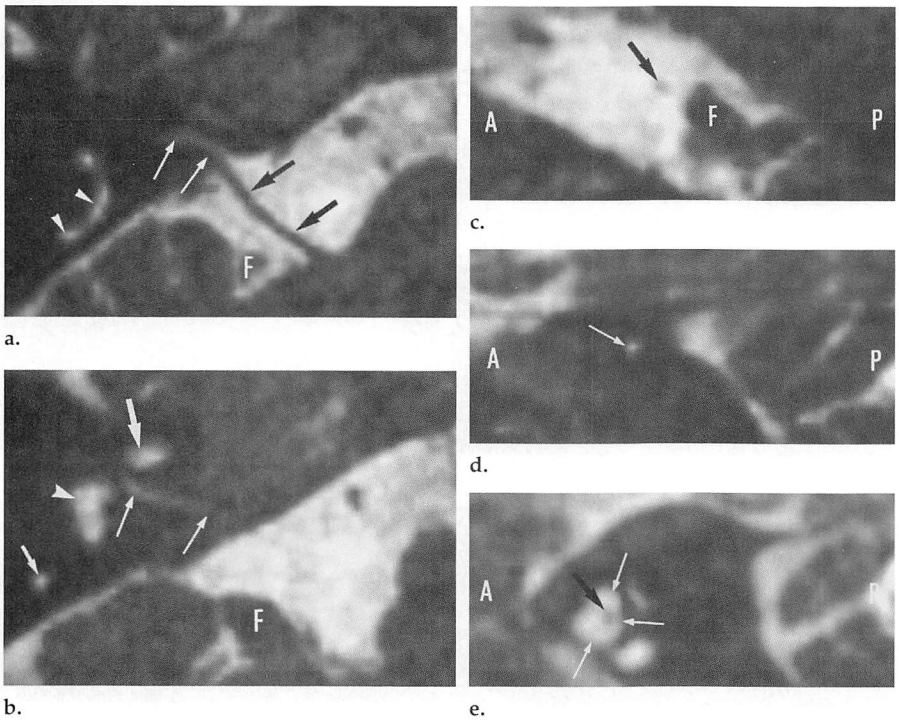

Figure 3. Patient 1. Type 1 malformation of the VCN (aplasia). **(a)** Axial 0.7-mm-thick 3DFT-CISS image (15/21, 65° flip angle) obtained through the upper part of the right stenotic internal auditory canal. Only very little cerebrospinal fluid can be seen in the stenotic internal auditory canal (white arrows), and it is impossible to demonstrate the presence or absence of nerves in such a narrow canal. Only one nerve, the facial nerve (black arrows), can be recognized in the cerebellopontine angle. *F* = flocculus, arrowheads = intralabyrinthine fluid in the common crus. **(b)** Axial 0.7-mm-thick 3DFT-CISS image (15/21, 65° flip angle) obtained through the lower part of the right stenotic internal auditory canal. Again, little cerebrospinal fluid is visible in the stenotic internal auditory canal (thin white arrows). High-signal-intensity intralabyrinthine fluid is seen in the cochlea (large white arrow), posterior semicircular canal (small white arrow), and vestibule (arrowhead). *F* = flocculus. **(c)** Parasagittal 3DFT-CISS reconstruction image obtained perpendicular to the course of the internal auditory canal and facial nerve at the level of the right cerebellopontine angle. At the level of the cerebellopontine angle, only the facial nerve (arrow) can be recognized anterior to the flocculus (*F*). In normal ears, two nerves are always present at this site (Figs 1, 2c). Therefore, parasagittal reconstruction images through the cerebellopontine angle are very reliable to demonstrate the absence of the VCN in patients with congenital deafness and normal facial nerve function. *A* = anterior, *P* = posterior. **(d)** Parasagittal 3DFT-CISS reconstruction image obtained perpendicular to the course of the internal auditory canal at the level of the middle third of the internal auditory canal shows the very narrow internal auditory canal filled with cerebrospinal fluid (arrow). It is impossible to recognize nerves in this narrow canal. *A* = anterior, *P* = posterior. **(e)** Parasagittal 3DFT-CISS reconstruction image obtained perpendicular to the course of the internal auditory canal at the level of the lateral third of the internal auditory canal. At the level of the fundus, the internal auditory canal is wider (white arrows), and this allows visualization of the facial nerve (black arrow); the three branches of the VCN are absent. *A* = anterior, *P* = posterior.

nerve and its superior and inferior vestibular branches is difficult to evaluate. Sometimes the bifurcation is seen only near the fundus of the internal auditory canal, and in the region just medial to the bifurcation, the nerve then becomes shaped like a figure eight and therefore has a large craniocaudal diameter. The diameters of the cochlear branch and the facial nerve were easier to depict inside the internal auditory canal on the parasagittal images and were more constant in size. Most frequently, the cochlear branch of the VCN was larger than the facial nerve, although the latter can be as large or even larger. The findings were more constant in the cerebellopontine angle, where the facial nerve and the VCN are found, and the latter was nearly always 1½–2 times larger than the facial nerve and was never smaller. These findings can be used as a reference when the nerves in the cerebellopontine angle and internal auditory canal have to be checked.

Embryologic Development

Aplasia of the complete VCN and aplasia or hypoplasia of its cochlear branch were demonstrated on MR images in seven patients (10 inner ears). These abnormalities occurred isolated or in association with a stenosis of the internal auditory canal and/or congenital malformation of the labyrinth. A possible explanation for these isolated and associated nerve abnormalities can be sought in the embryologic development of the labyrinth and VCN.

The development of the human cochlea starts with the appearance of the otic placode at the third embryonic week. This placode transforms into the otic vesicle that gives rise to the endolymphatic duct, the utriculus, sacculus, semicircular canals, and cochlea. At 9 weeks, the cochlear windings are fully developed and the appearance of the neural epithelium has started. Neuroblasts of the cochlear ganglion separate from the otic epithelium. Fibers from these ganglion cell bodies grow peripherally back into the otic epithelium and centrally into the brain stem (15). The first afferent fibers entering the undifferentiated otic epithelium are seen at 9–10 weeks (16). In the avian embryo, an abundant neuronal population invades the epithelium (17,18). This is followed by the disappearance of many redundant fibers, which may lead to a 25% reduction in the number of fibers. This reorganization is called "neural stabilization" (17). Although it has been thought that the cochlear development or differentiation depends on the innervation, this has been proved not to be the case. Explants of chicken otic vesicles that lack neuronal fibers give rise to inner ear sensory structures with normal morphologic features in vitro. This implies that the inner ear development is not dependent on any neuronal trigger or stimulus or trophic effect (19). Also, the differentiation of the hair cells is controlled by location-specific cues that originate in the ear itself. Conversely, the developing inner ear appears to have an important trophic effect on the survival and the cytodifferentiation of the afferent neurones. The otic vesicle releases a nerve growth factor–like substance that is essential for the survival of the neurones and for "neuronal stabilization" (18).

These data can explain why the VCN or its cochlear branch can be absent in patients with an abnormal or absent cochlea. It is equally conceivable that a disturbance in the trophic effect that the cochlea exerts on the cochlear neurones may result in a well-developed cochlea without a surviving cochlear nerve. The association of an absent VCN and a stenosis of the internal auditory canal is not explained by these findings, but a possible hypothesis is that a normal internal auditory canal is formed only in the presence of a normal nerve.

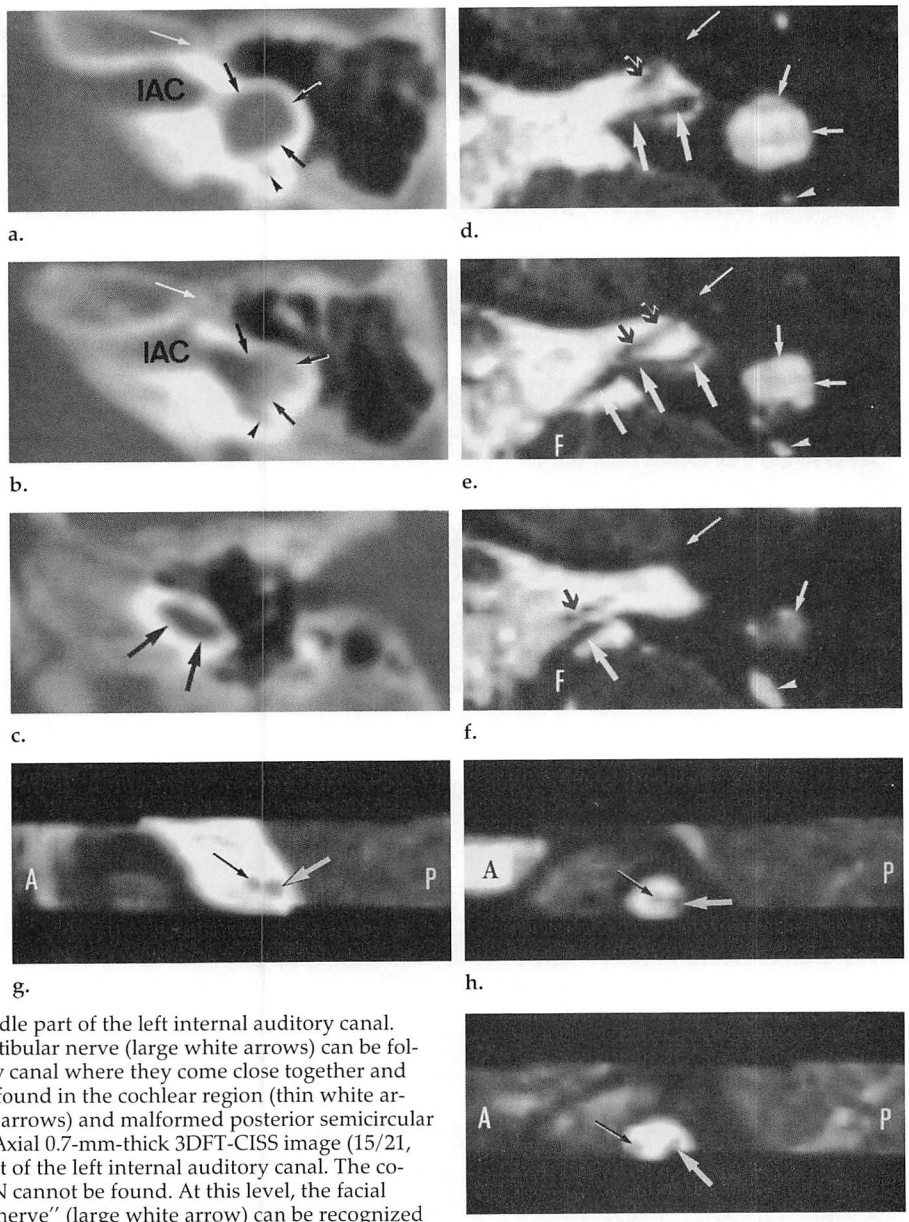

Figure 4. Patient 3. Type 2A malformation of the VCN (common VCN with aplasia of its cochlear branch in the presence of a labyrinthine malformation). **(a)** Axial 1.5-mm-thick CT scan of the left inner ear obtained through the upper part of the internal auditory canal shows only a single cavity (black arrows). The cochlea cannot be found at its normal site (white arrow), and in this patient, the cochlea and the vestibule formed a single or "common cavity." A partially developed and malformed posterior semicircular canal (arrowhead) can be seen. *IAC* = internal auditory canal. **(b)** Axial 1.5-mm-thick CT scan of the left inner ear obtained through the lower part of the internal auditory canal. The absence of the cochlea (white arrow) and the presence of a common cavity (black arrows) and a partially developed posterior semicircular canal (arrowhead) are confirmed at this level. *IAC* = internal auditory canal. **(c)** Axial 1.5-mm-thick CT scan of the left inner ear obtained through the base of the abnormal labyrinth. At this level, an oval inferior extension of the common cavity can be recognized (arrows) and mimics a basal turn of a cochlea. **(d)** Axial 0.7-mm-thick 3DFT-CISS image (15/21, 65° flip angle) obtained through the upper part of the left internal auditory canal. The facial nerve (black arrow) and a vestibular nerve (large white arrows) can be depicted just under the roof of the internal auditory canal. No fluid is seen at the site where one normally finds the cochlea (thin white arrow), and a fluid-filled common cavity (small white arrows) and posterior semicircular canal (arrowhead) are the only labyrinthine structures that can be visualized. The upper part of the posterior semicircular canal was missing on the adjacent images (not shown) made higher through the inner ear. **(e)** Axial 0.7-mm-thick 3DFT-CISS image (15/21, 65° flip angle) obtained through the middle part of the left internal auditory canal. Both the facial nerve (black arrows) and the vestibular nerve (large white arrows) can be followed toward the porus of the internal auditory canal where they come close together and touch the posterior lip of the porus. No fluid is found in the cochlear region (thin white arrow). A fluid-filled common cavity (small white arrows) and malformed posterior semicircular canal (arrowhead) are noted. *F* = flocculus. **(f)** Axial 0.7-mm-thick 3DFT-CISS image (15/21, 65° flip angle) obtained through the inferior part of the left internal auditory canal. The cochlear and inferior vestibular branch of the VCN cannot be found. At this level, the facial nerve (black arrow) and a "common vestibular nerve" (large white arrow) can be recognized in the cerebellopontine angle just anterior to the flocculus (*F*). The nerve is called a common vestibular nerve because no separate superior and inferior branches of the VCN are present in this patient. The absence of fluid in the normal region of the cochlea (thin white arrow) and the presence of a fluid-filled abnormal broad posterior semicircular canal (arrowhead) and "common cavity" (small white arrow) are confirmed. **(g)** Parasagittal 3DFT-CISS reconstruction image obtained at the level of the left cerebellopontine angle. Two nerves can be seen in the cerebellopontine angle, and the VCN (white arrow) is larger than the facial nerve (black arrow), which is a normal finding. *A* = anterior, *P* = posterior. **(h)** Parasagittal 3DFT-CISS reconstruction image obtained at the level of the middle third of the left internal auditory canal. At this level, the cochlear branch of the VCN is missing, and only a common VCN (white arrow) posteriorly and a facial nerve (black arrow) can be recognized. *A* = anterior, *P* = posterior. **(i)** Parasagittal 3DFT-CISS reconstruction image obtained at the level of the lateral third of the left internal auditory canal. Near the fundus of the internal auditory canal, the common VCN (white arrow) is still seen instead of the three branches of the VCN that should be seen at this level. The facial nerve (black arrow), seen in the anterior part of the internal auditory canal, has an abnormal low position inside the internal auditory canal. *A* = anterior, *P* = posterior.

Therefore, a disturbance in the trophic effect of the cochlea can result in loss of too many or all neuronal fibers, and in these patients, the internal auditory canal formed around the initial neuronal fibers will not develop further and eventually will be stenotic.

Classification Proposal

The MR findings in the seven patients with aplasia or hypoplasia of the cochlear branch of the VCN were in accordance with the clinical findings (Table) but as yet cannot be confirmed with surgery or at pathologic examination. The authors believe that the presented cases represent different stages or grades of developmental anomalies of the VCN. According to the CT, MR imaging, and clinical findings and with respect to embryologic knowledge, we propose the following classification.

Type 1: Aplasia of the VCN Associated with Stenosis of the Internal Auditory Canal

Bilateral stenotic internal auditory canals (patient 1) and a left-sided stenosis (patient 2) were recognized on CT scans and on the axial 3DFT-CISS images and parasagittal 3DFT-CISS reconstruction images. Both patients had normal labyrinths. It was, however, impossible to look for nerves in the extremely narrow internal audi-

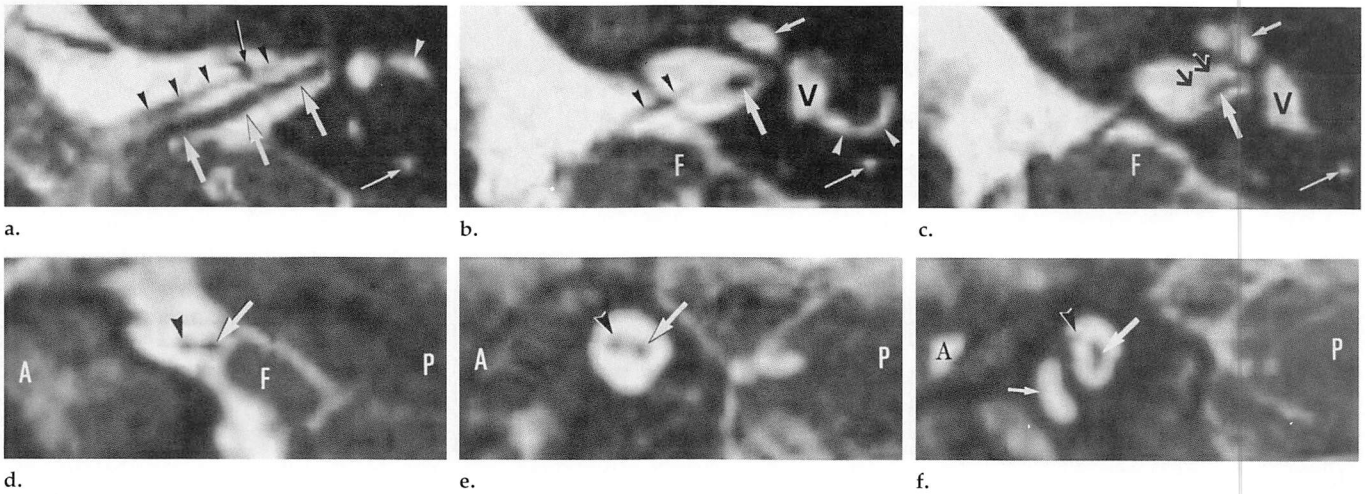

a. b. c.

d. e. f.

Figure 5. Patient 5. Type 2B malformation of the VCN (common VCN with aplasia of its cochlear branch in the presence of a normal labyrinth). **(a)** Axial 0.7-mm-thick 3DFT-CISS image (15/21, 65° flip angle) obtained through the upper part of the left internal auditory canal. The facial nerve (black arrowheads) and a common VCN (large white arrows) are seen high in the internal auditory canal; a vascular loop (black arrow) is crossing the facial nerve deep in the internal auditory canal. Fluid is noted in the lateral (white arrowhead) and posterior (white arrow) semicircular canals. **(b)** Axial 0.7-mm-thick 3DFT-CISS image (15/21, 65° flip angle) obtained through the middle part of the left internal auditory canal. The facial nerve (black arrowheads) can be followed toward the cerebellopontine angle, and part of the "common VCN" (large white arrow) is depicted. A cochlear branch of the VCN cannot be demonstrated. High-signal-intensity intralabyrinthine fluid is noted in the cochlea (small white arrow) and lateral (white arrowheads) and posterior (thin white arrow) semicircular canals. *F* = flocculus, *V* = vestibule. **(c)** Axial 0.7-mm-thick 3DFT-CISS image (15/21, 65° flip angle) obtained through the inferior part of the left internal auditory canal. Part of the common VCN (large white arrow) is still visible near the floor of the internal auditory canal. The cochlear branch of the VCN is again absent (black arrows). Fluid is noted inside the cochlea (small white arrow) and the posterior semicircular canal (thin white arrow). *F* = flocculus, *V* = vestibule. **(d)** Parasagittal 3DFT-CISS reconstruction image obtained perpendicular to the course of the nerves at the level of the left cerebellopontine angle. The facial nerve (arrowhead) and the VCN (arrow) have the same size at the level of the cerebellopontine angle, which is a rare finding in normal inner ears. Moreover, in this patient, the VCN was twice as large as the facial nerve on the opposite normal side (not shown), which supports the diagnosis of hypoplasia of the VCN. *A* = anterior, *F* = flocculus, *P* = posterior. **(e)** Parasagittal 3DFT-CISS reconstruction image obtained perpendicular to the course of the nerves at the level of the middle third of the left internal auditory canal. The cochlear branch of the VCN cannot be recognized, confirming the findings in **b** and **c**. Therefore, the two nerves seen on this image must be the facial nerve (arrowhead) anteriorly and a common VCN (arrow) posteriorly. *A* = anterior, *P* = posterior. **(f)** Parasagittal 3DFT-CISS reconstruction image perpendicular to the course of the nerves at the level of the lateral third of the left internal auditory canal. Near the fundus of the internal auditory canal, the facial nerve (arrowhead) occupies its normal position. However, a separate superior and inferior vestibular branch of the common VCN and a cochlear branch cannot be demonstrated. Instead, a single common VCN continues deep in the internal auditory canal and gets larger in craniocaudal diameter (large arrow) near the fundus, explaining why this nerve could be identified on three contiguous 0.7-mm-thick axial images **a–c**. *A* = anterior, *P* = posterior, small arrow = high-signal-intensity intralabyrinthine fluid in the cochlea.

tory canals in these two patients (Fig 3). Nevertheless, the cerebellopontine angle could still be evaluated in these patients, and both the axial and reconstructed parasagittal gradient-echo images showed the presence of a single nerve—the facial nerve. As already mentioned, the absence of the VCN in the presence of a normal cochlea can be explained by a disturbance of the trophic effect (nerve growth factor) that the cochlea exerts on the cochlear neurones (18). The hypothesis for the associated stenosis of the internal auditory canal is that the absence of a normally developing VCN causes the stenosis of the internal auditory canal. The internal auditory canal is formed around the neuronal fibers of the VCN, but these fibers can again disappear when there is a disturbance in the trophic effect of the cochlea (nerve growth factor) on these fibers. This excessive loss of fibers or loss of all fibers probably results in an arrest of the development of the internal auditory canal. A separate canal for the facial nerve was detected on CT scans and gradient-echo MR images in patient 2. This shows that abnormal development of the nerves can even be associated with more severe and rare abnormalities of their canals.

In these patients, the findings on the parasagittal 3DFT-CISS reconstruction images made through the cerebellopontine angle are very reliable in the exclusion or confirmation of aplasia of the VCN. Partial volume effects cannot explain the disappearance of a nerve in this plane, and in normal inner ears, both the facial nerve and VCN were always visible anterior to the flocculus (Fig 2). Therefore, it is advisable to look for aplasia of the VCN at this level in patients with congenital hearing loss and associated stenosis of one or both internal auditory canals.

The MR demonstration of the absence of a VCN might predict that a cochlear implant will not work. Nevertheless, it could be interesting to perform an electric promontory stimulation test and functional MR imaging of the auditory cortex to exclude the presence of very thin cochlear fibers, too thin to be detected on MR images. However, it seems unlikely that a completely invisible VCN on MR images would possess enough fibers to result in worthwhile hearing.

Type 2: Common VCN with Aplasia or Hypoplasia of Its Cochlear Branch

Type 2A: type 2 in the presence of a labyrinthine malformation.—In two patients (patients 3 and 4), the cochlea and vestibule formed a single, large, fluid-filled cavity, known as a common cavity (20). They also had associated malformations of the semicircular canals (Table). In both patients, the axial gradient-echo images and the parasagittal reconstruction images showed that the cochlear branch of the VCN was absent (Fig 4). As mentioned above, the absence of a normal developing cochlea can impede the survival or cytodifferentiation of the afferent neurons (cochlear branch) and can explain this combination of malformations. The absence of the cochlear branch was initially over-

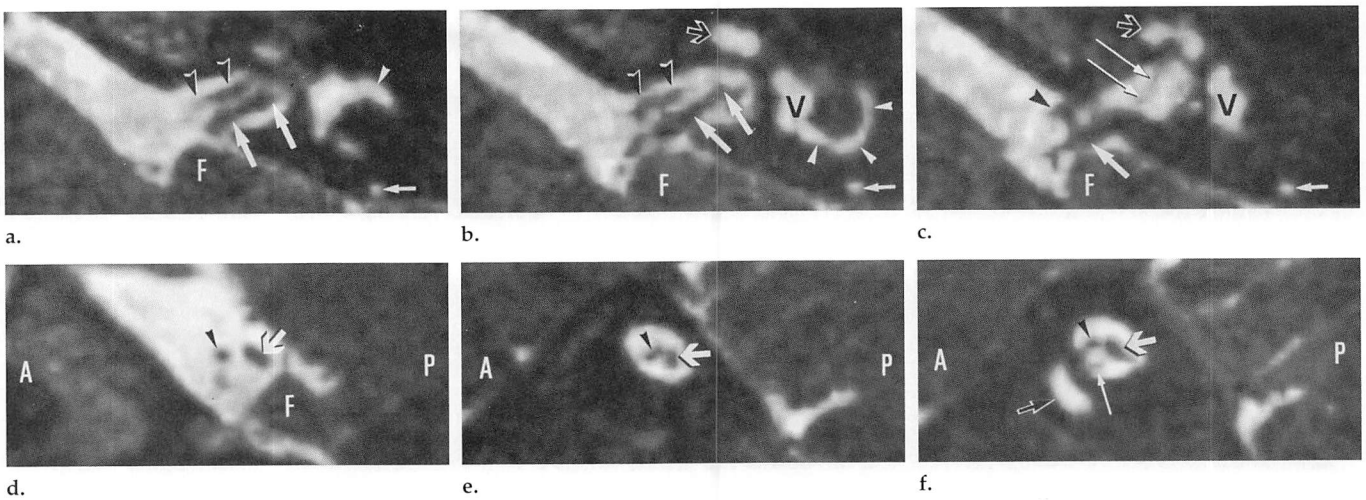

Figure 6. Patient 7. Type 2B malformation of the VCN (common VCN with hypoplasia of its cochlear branch in the presence of a normal labyrinth). **(a)** Axial 0.7-mm-thick 3DFT-CISS image (15/21, 65° flip angle) obtained through the upper part of the left internal auditory canal. The facial nerve (black arrowheads) and a common VCN (large arrows) are seen parallel to one another in the upper part of the internal auditory canal. Intralabyrinthine fluid is noted inside the lateral (white arrowhead) and posterior (small arrow) semicircular canals. *F* = flocculus. **(b)** Axial 0.7-mm-thick 3DFT-CISS image (15/21, 65° flip angle) through the middle part of the left internal auditory canal. The facial nerve can be followed toward the porus of the internal auditory canal (black arrowheads), and the common VCN (large white arrows) is still visible in the internal auditory canal and near the porus. High-signal-intensity fluid is seen in the cochlea (black arrow), the lateral semicircular canal (white arrowheads), the posterior semicircular canal (small white arrow), and the vestibule (*V*). *F* = flocculus. **(c)** Axial 0.7-mm-thick 3DFT-CISS image (15/21, 65° flip angle) obtained through the inferior part of the left internal auditory canal. The facial nerve (arrowhead) and the common VCN (large white arrow) are seen in the cerebellopontine angle on this image made just above the floor of the internal auditory canal. A very thin cochlear branch of the VCN (thin white arrows) can be depicted deep in the internal auditory canal, compatible with a hypoplastic cochlear branch. Intralabyrinthine fluid is noted inside the cochlea (black arrow), posterior semicircular canal (small white arrow), and vestibule (*V*). *F* = flocculus. **(d)** Parasagittal 3DFT-CISS reconstruction image obtained perpendicular to the course of the nerves at the level of the left cerebellopontine angle. The common VCN (arrow) is twice as large as the facial nerve (arrowhead). This is a normal finding at this site, and therefore no malformation is suspected on this image. *A* = anterior, *F* = flocculus, *P* = posterior. **(e)** Parasagittal 3DFT-CISS reconstruction image obtained perpendicular to the course of the nerves at the level of the middle third of the left internal auditory canal. Only two nerves, the facial nerve (arrowhead) and a common VCN (arrow), are recognized. A separate cochlear branch, normally already visible at this site, is absent. *A* = anterior, *P* = posterior. **(f)** Parasagittal 3DFT-CISS reconstruction image obtained perpendicular to the course of the nerves at the level of the lateral third of the left internal auditory canal. Near the fundus of the internal auditory canal, the facial nerve (arrowhead) is seen in its normal position high and anterior in the internal auditory canal. A common vestibular nerve (thick white arrow) is seen instead of two separate branches deep in the internal auditory canal, and a very thin hypoplastic cochlear branch (thin white arrow) is depicted. Deep in the internal auditory canal, the cochlear branch can be smaller than the facial nerve but the size always remains close to the size of the facial nerve in normal inner ears. This is not the case in this patient. Moreover, the diameter of the cochlear branch of the opposite normal inner ear was larger than the diameter of the facial nerve (not shown). This finding supports the diagnosis of a hypoplastic cochlear branch of the VCN. *A* = anterior, *P* = posterior, black arrow = high-signal-intensity intralabyrinthine fluid in the cochlea.

looked on the axial MR images of one of these patients (patient 3), and at that time, parasagittal reconstruction images were not made. The diagnosis was made only several months later when the images were reviewed for a study on congenital malformations. In the meantime, electric stimulation of the left ear had elicited clear subjective hearing sensation, and as a consequence, the ear surgeon (F.E.O.) placed a cochlear implant (LAURA; Antwerp Bionic Systems, Antwerp, Belgium) into the inferior part of the common cavity, which looked like a basal turn of the cochlea (Fig 4c). The postoperative electroaudiogram was within the normal range and stable throughout the 6-month postoperative period, and the child showed clear signs of auditory progress (voice control, auditory behavior). The most probable explanation or hypothesis is that the single common VCN probably carries some fibers projecting into the auditory cortex. These results make it, of course, difficult to make a decision in the second patient (patient 4), with similar malformations on both sides and bilateral stenoses of the internal auditory canal. The results of the electric promontory stimulation can guide the surgeon, and in the future, functional MR imaging of the auditory cortex might become the technique of choice. Only this imaging modality has the potential to demonstrate whether "cochlear fibers" connect an abnormal labyrinth with the brain stem and auditory cortex, even in the absence of a cochlear branch of the VCN.

Type 2B: type 2 in patients with a normal labyrinth.—Three patients presented with completely normal labyrinths and internal auditory canals. The axial and parasagittal gradient-echo images showed an absent cochlear branch of the VCN in two patients (patients 5 and 6), and in these patients, the common vestibular nerve could be followed to the fundus of the internal auditory canal without a clear bifurcation or a very late (not visible on MR images due to partial volume effect with the fundus) bifurcation in a superior and inferior vestibular nerve (Fig 5). In a third patient (patient 7), a very thin cochlear branch could be seen on the axial and parasagittal gradient-echo images (Fig 6). In these three patients, a disturbance in the trophic effect (nerve growth factor) that the cochlea exerts on the cochlear neurones could once again explain the hypoplasia or complete absence of the cochlear branch of the VCN. Of course, these findings had no clinical consequences as these three patients had a normal functioning contralateral ear; nevertheless, the MR findings correlated well with the unilateral hearing loss. However, in patients with normal labyrinths and bilateral aplasias of the cochlear branch of the VCN, electric promontory stimulation and/or functional MR imaging should be used as a selection tool for cochlear implant candidacy.

The absence of the cochlear branch can be recognized on thin-section gradient-echo images, although once again parasagittal reconstruction images are mandatory to confirm the findings seen on the axial images. The danger exists that the cochlear branch lies adjacent to the floor of the internal auditory canal and is therefore not seen on the axial gradient-echo images due to partial volume effects. The parasagittal plane is better suited to study this region and can be used to exclude partial volume effects. The diagnosis of hypoplasia of the cochlear branch is more difficult. In three of the 20 normal inner ears, the cochlear branch of the VCN inside the internal auditory canal was smaller than the facial nerve. But even in these cases, the diameters of both nerves were nearly the same. In patient 7, the diameter of the cochlear branch was much smaller than the diameter of the facial nerve, whereas on the opposite normal side the cochlear branch was much larger than the facial nerve.

Type 3?: Presence of a Common VCN with Aplasia or Hypoplasia of the Vestibular Branch(es)

Theoretically, a third type of VCN aplasia or hypoplasia with only absence of the vestibular branches but with a normal cochlear branch could be conceived. To our knowledge, such a type of VCN malformation has not yet been detected on MR images. Since the vestibule develops at an earlier stage than the cochlea, one may expect that a vestibular malformation will always lead to an associated cochlear malformation. In such a case, a type 1 aplasia would be the result. Therefore, the authors speculate that an isolated aplasia of the vestibular branch or type 3 aplasia of the VCN may not exist. ■

References

1. Mark AS, Seltzer S, Nelson-Drake J, Chapman JC, Fitzgerald DC, Gulya AJ. Labyrinthine enhancement on Gd-MRI in patients with sudden deafness and vertigo: correlation with audiologic and electronystagmographic studies. Ann Otol Rhinol Laryngol 1992; 101:459–464.
2. Mark AS, Fitzgerald D. Segmental enhancement of the cochlea on contrast-enhanced MR: correlation with the frequency of hearing loss and possible sign of perilymphatic fistula and autoimmune labyrinthitis. AJNR 1993; 14:991–996.
3. Mark AS. Contrast-enhanced magnetic resonance imaging of the temporal bone. Neuroimaging Clin North Am 1994; 4:117–131.
4. Casselman JW, Kuhweide R, Dehaene I, Ampe W, Devlies F. Magnetic resonance examination of the inner ear and cerebellopontine angle in patients with vertigo and/or abnormal findings at vestibular testing. Acta Otolaryngol 1994; 513(suppl): 15–27.
5. Casselman JW. Temporal bone imaging. Neuroimaging Clin North Am 1996; 6:265–289.
6. Casselman JW, Kuhweide R, Ampe, et al. Inner ear malformations in patients with sensorineural hearing loss: detection with gradient-echo (3DFT-CISS) MRI. Neuroradiology 1996; 38:278–286.
7. Klein HM, Bohndorf K, Hermes H, et al. Computed tomography and magnetic resonance imaging in the preoperative work-up for cochlear implantation. Eur J Radiol 1992; 15:89–92.
8. Marsot-Dupuch K, Meyer B. Imagerie des implants cochléaires. In: Bourjat P, Veillon F, eds. Imagerie radiologique tête et cou. 1st ed. Paris, France: Editions Vigot, 1995; 147–159.
9. Harnsberger HR, Dart DJ, Parkin JL, Smoker WRK, Osborn AG. Cochlear implant candidates: assessment with CT and MR imaging. Radiology 1987; 164:53–57.
10. Casselman JW, Kuhweide R, Deimling M, Ampe W, Dehaene I, Meeus L. Constructive interference in steady state-3DFT MR imaging of the inner ear and cerebellopontine angle. AJNR 1993; 14:47–57.
11. Schmalbrock P, Brogan MA, Chakeres DW, Hacker VA, Ying K, Clymer BD. Optimization of submillimeter-resolution MR imaging methods for the inner ear. JMRI 1993; 3:451–459.
12. Tien RD, Felsberg GJ, Macfall J. Three dimensional MR gradient recalled echo imaging of the inner ear: comparison of FID and echo imaging techniques. JMRI 1993; 11:429–435.
13. Tanioka H, Shirakawa T, Machida T, Sasaki Y. Three-dimensional reconstructed MR imaging of the inner ear. Radiology 1991; 178:141–144.
14. Tien R, Felsberg GJ, Macfall J. Fast spin-echo high-resolution MR imaging of the inner ear. AJR 1992; 159:395–398.
15. Hemond SG, Delanty FJ. Formation of the cochlea in the chicken embryo: sequence of innervation and localization of basal lamina–associated molecules. Brain Res Dev Brain Res 1991; 61:87–90.
16. Pujol R, Lavigne-Rebillard M, Uziel A. Development of the cochlea. Acta Otolaryngol Suppl (Stockh) 1991; 482:7–12.
17. Lefebvre PP, Weber T, Rigo JM, et al. Interactions neuronotrophiques dans l'oreille interne en développement. Acta Otorhinolaryngol Belg 1989; 43:403–409.
18. Lefebvre PP, Leprince P, Weber T, Rigo JM, Delree P, Moonen G. Neuronotrophic effect of developing otic vesicle on cochleovestibular neurons: evidence for nerve growth factor involvement, Brain Res 1990; 507:254–260.
19. Van De Water TR. Effects of removal of the statoacoustic ganglion complex upon the growing otocyst. Ann Otol Rhinol Laryngol 1976; 85:2–31.
20. Jackler RK, Luxford WM, House WF. Congenital malformations of the inner ear: a classification based on embryogenesis. Laryngoscope 1987; 97:2–14.

Book Review

Radiologische Anatomie und Topographie des Halses: CT, MR, Röntgenbild, Sialographie und Pharyngographie [Radiologic Anatomy and Topography of the Neck Region: CT, MR, Radiography, Sialography, and Pharyngography]

Andreas Prescher, MD, and Klaus Bohndorf, MD

Stuttgart, Germany: Thieme Verlag, 1996. ISBN 3-13-106721-7. Hardcover, DM 198; pp 214; 180 figures.

The authors of this book undertook the difficult task of reviewing the normal anatomy of the head and neck in its entirety. The book is divided into 10 chapters, which include topics such as cervical spine anatomy, computed tomographic (CT) anatomy of the neck, magnetic resonance (MR) imaging anatomy of the neck, vascular anatomy, nerves of the neck, lymph node anatomy, ligaments of the cervical spine, salivary glands, functions of the pharynx and larynx, and fascial layers/anatomic spaces of the neck.

For the most part, the chapters are a focused look at the particular anatomic regions of interest with imaging (CT, MR imaging, plain radiography, and contrast material–enhanced studies [salivary glands and pharynx/larynx]) and corresponding labeled drawings. In a few of the chapters, such as the ones that cover vascular anatomy, lymph nodes, and ligamentous anatomy, only labeled drawings are used. Brief discussions of the anatomy are found in a few chapters; however, for the most part this is an anatomy atlas.

A good, but brief, discussion of the functions of the pharynx and larynx and sialography were also included. These studies are not commonly performed, but it is often difficult to find related references.

The detailed anatomic drawings are of very good quality with extensive labeling of structures. Most of the drawings are made directly from the corresponding imaging studies, which are also of good quality. References are as you would expect in an anatomy atlas; they range from the 1930s to several more recent articles from the 1990s. Since all structures are labeled in medical Latin (ie, international terminology), the book is accessible to medical readers of any language capability. Brief text is in German.

I believe the authors of this book have done a very good job in putting together a succinct synopsis of the difficult subject of head and neck anatomy. The book is well suited as a primer in this subject for the beginning radiology resident or otolaryngology resident or perhaps a quick reference for the more experienced radiologist who does not commonly image this area. For those who are more frequently involved with imaging of this area and need a more in-depth discussion, several more extensive textbooks are available.

Reviewed by John C. Egelhoff, DO